The Impact of Janus Nanoparticles on the Compatibilization of Immiscible Polymer Blends under Technologically Relevant Conditions

Ronak Bahrami,[†,∥] Tina I. Löbling,[‡,∥] André H. Gröschel,[§] Holger Schmalz,[‡] Axel H. E. Müller,[*,‡,⊥] and Volker Altstädt[*,†]

[†]Fakultät für Ingenieurwissenschaften, [‡]Makromolekulare Chemie II, Universität Bayreuth, 95440 Bayreuth, Germany, [§]Molecular Materials, Department of Applied Physics, School of Science, Aalto University, 02150 Espoo, Finland, and [⊥]Institut für Organische Chemie, Johannes Gutenberg-Universität Mainz, D-55099 Mainz, Germany. [∥]These authors contributed equally to this work.

ABSTRACT Several hundred grams of Janus nanoparticles ($d \approx 40$ nm) were synthesized from triblock terpolymers as compatibilizers for blending of technologically relevant polymers, PPE and SAN, on industry-scale extruders. The Janus nanoparticles (JPs) demonstrate superior compatibilization capabilities compared to the corresponding triblock terpolymer, attributed to the combined intrinsic properties, amphiphilicity and the Pickering effect. Straightforward mixing and extrusion protocols yield multiscale blend morphologies with "raspberry-like" structures of JPs-covered PPE phases in a SAN matrix. The JPs densely pack at the blend interface providing the necessary steric repulsion to suppress droplet coagulation during processing. We determine the efficiency of JP-compatibilization by droplet size evaluation and find the smallest average droplet size of $d \approx 300$ nm at 10 wt % of added compatibilizer, whereas at 2 wt %, use of JPs is most economic with reasonable small droplets and narrow dispersity. In case of excess JPs, rheological properties of the system is changed by a droplet network formation. The large-scale synthesis of JPs, the low required weight fractions and their exceptional stability against extensive shear and temperature profiles during industrial extrusion process make JP promising next generation compatibilizers.

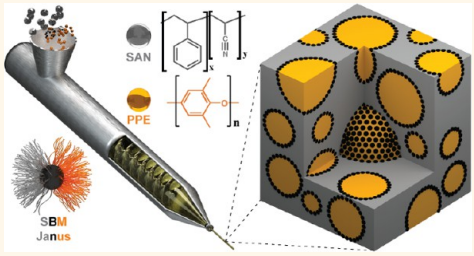

KEYWORDS: Janus particles · materials science · nanoparticles · polymer blends · self-assembly

The blending of polymers is a well-established and versatile concept to economically unify desirable material properties of multiple components within new materials and builds the foundation of an entire industry.[1−3] The inherent immiscibility of polymers usually demands the careful design of blend recipes, processing conditions and/or the addition of compatibilizers to control the blend morphology.[4,5] Compatibilizers may add further functionality and range from organic molecules to block and graft copolymers,[6,7] nanoparticles[8−11] and carbon based reinforcements.[12,13] Thereby, nanoparticle reinforced composites have evolved into a vivid research field owing to the selective localization of particles and thus functional matter at the blend interface.[14−17] In that regard, Janus nanoparticles (JPs) have received much less attention, despite their known exceptional performance in applications that specifically rely on the minimization of interfacial energies (emulsions, suspensions, melts).[18−21] JPs are the colloidal analogue of surfactants and amphiphilic block copolymers and feature different physical properties on opposing hemispheres.[22−24] The combination of amphiphilicity and particulate character (Pickering effect) favors strong and selective adsorption to interfaces. Among others, this is considered challenging when applying nanoparticle compatibilizers in polymer melts.[25,26] Previous work on polystyrene/poly(methyl methacrylate) (PS/PMMA) blends compatibilized by JPs with matching PS and PMMA hemispheres served as an ideal small-scale model for comprehensive studies on JP location, blending efficiency and morphological evolution.[27] Since then, only a handful of theoretical works advanced this prospective research field.[28−30] Studies involving JPs mostly focus on polymer blends that allow convenient handling

* Address correspondence to altstaedt@uni-bayreuth.de, axel.mueller@uni-mainz.de.

Received for review May 15, 2014 and accepted September 11, 2014.

Published online September 11, 2014
10.1021/nn502662p

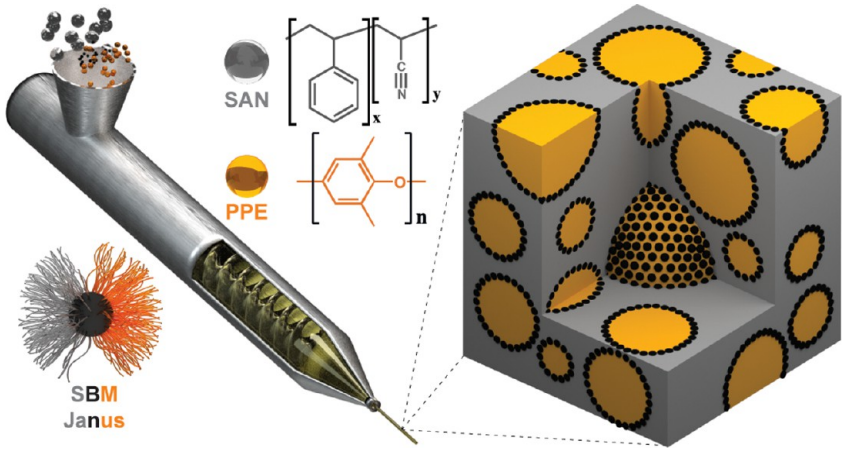

Figure 1. Processing of polymer blends using Janus nanoparticles (JPs) as compatibilizer. During extrusion of the polymer melt, JPs (black dots) compatibilize and stabilize PPE droplets (yellow) within the SAN matrix (gray).

(in experiments and calculations) as to understand underlying mechanisms, while studies on blends with material properties appealing for practical applications have remained beyond laboratories' reach.

Poly(2,6-dimethyl-1,4-phenylene ether) (PPE) blended with poly(styrene-*co*-acrylonitrile) (SAN) is such a system of technological relevance. PPE is usually blended with PS, since they are fully miscible, to facilitate its processability. Yet, the need for a modified system, preferably based on PS or its copolymers, with better chemical stability and higher T_g (like SAN) is of high scientific interest. The new blend would combine the heat resistance and dimensional stability of PPE with the stiffness and easy processability of SAN; however, the miscibility of the system depends strongly on the acrylonitrile content of the SAN phase. Almost all commercially available SAN polymers have AN contents between 18 and 35 wt %, whereas above 12.4 wt % the PPE/SAN system is immiscible.[31] In this case, the high surface energy and the low tendency of PPE to form interfaces with SAN cause PPE droplets to rapidly coagulate during extrusion, rendering compatibilizers an essential part of the blend recipe. In earlier studies, we showed that the ABC triblock terpolymer polystyrene-*block*-polybutadiene-*block*-poly(methyl methacrylate) (SBM) efficiently compatibilizes this blend since PS is compatible with PPE and PMMA with SAN.[32−35] The soft PB middle block forms low modulus droplets located at the interface and may serve to dissipate energy. We hypothesize that the use of JPs made from SBM triblock terpolymers could distinctly improve the blend microstructure and outperform the triblock terpolymer due to the superior interfacial activity of amphiphilic particles. So far, JPs have not been studied as compatibilizers in industry-scale blend systems due to severe challenges in the up-scaling of particle production (typically solved for μg to mg amounts).[21,36] In general, there is a lack of available JP types that are able to operate on the relevant size scale, *i.e.*, particles should be considerably smaller (<100 nm) than the to-stabilize blend polymer droplets (<1 μm). It is thus not surprising that JPs are still considered an exotic class of material, merely suited for specialized research and not appropriate for large-scale applications.

Here, we present the first studies on the performance of Janus nanoparticles in technologically relevant polymer blend systems in industry-scale blending equipment using 200 g of SBM JPs for the compatibilization of several kilograms of PPE and SAN (Figure 1). We show that despite high shear rates during melt processing JPs quantitatively adsorb at the blend interface and we derive mechanistic explanations for the morphological impact of JPs on the studied polymer blend system. Both are key aspects for the implementation of JPs as compatibilizers in industry-scale processes.

RESULTS AND DISCUSSION

We recently reported on the solution-based synthesis of nanosized JPs, which opens the way to significantly larger quantities of JPs.[37] The JPs for this study were prepared from a triblock terpolymer of the composition $S_{40}B_{20}M_{40}^{108}$ (subscripts denote block weight fractions and superscript overall molecular weight in kg/mol) according to a modified recipe from ref 37 (see Supporting Information) yielding 100 g JPs in a single batch (Supporting Information Figure S1). The JPs feature a cross-linked PB core and equally sized PS/PMMA hemispheres (Supporting Information Figures S2 and S3). The polymer chains of the hemispheres are above the critical entanglement lengths, M_c, with $M_{n,PS}$ = 42 kg/mol ($M_{c,PS}$ = 34 kg/mol)[38] and $M_{n,PMMA}$ = 42 kg/mol ($M_{c,PMMA}$ = 18 kg/mol),[39] ensuring sufficient interaction between JPs and the blended polymers. In a typical blend experiment, 540 g of PPE powder and 360 g of SAN polymer pellets were dry-mixed together with 100 g of JPs to yield a blend ratio of PPE/SAN 60/40 (w/w) containing 10 wt % JPs as compatibilizer. This particular blend ratio has a

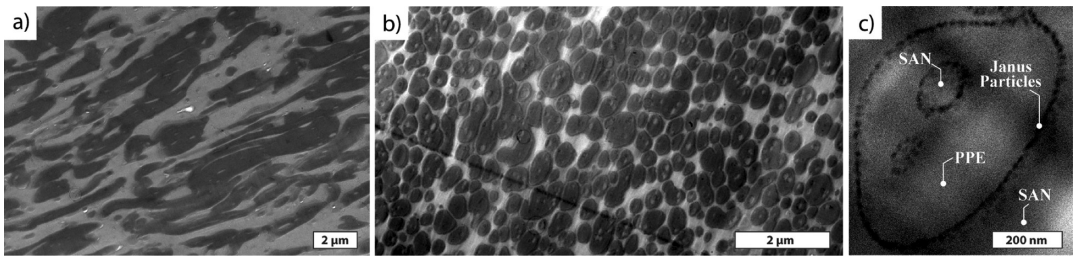

Figure 2. Droplet morphology of the PPE (dark)/SAN (bright) blend (60/40 w/w), as neat blend and compatibilized with 10 wt % of SBM JPs. (a) TEM overview of the PPE/SAN (60/40 w/w) blend without and (b and c) with compatibilization. The neat blend system shows irregular, elongated, and fused droplets, whereas small drop morphology occurs with 10 wt % JPs (b). The TEM magnification (c) of one PPE droplet shows JPs as black dots exclusively located at the PPE/SAN blend interface. PB cores of JPs were selectively stained with OsO_4 to increase the contrast.

well-processable medium viscosity and demonstrated convincing blend performance in earlier studies.[13,32,33,40] After optimizing process parameters such as screw speed on the neat blend, all mixtures were extruded on a Brabender DSE twin-screw extruder at fixed nozzle temperature of 245 °C, at constant screw speed of 85 rpm and constant throughput of 1 kg/h (details are given in the Experimental Section).

To analyze the blend morphology, scanning electron microscopy (SEM) and transmission electron microscopy (TEM) were used. For TEM imaging, ultrathin sections (thickness <100 nm) were cut from the blend granules after extrusion (Figure 2). We find a substantial improvement of the blend homogeneity after addition of 10 wt % JPs (Figure 2b) compared to the neat blend system (Figure 2a). The neat blend shows elongated, ill-shaped droplets that frequently coagulate and resemble a co-continuous phase (parallel to extrusion direction), whereas the JP blend shows an entirely different morphology of small droplets. The morphology in Figure 2b shows small PPE droplets (dark) embedded in a continuous SAN matrix (bright). Strikingly, the droplets are able to pack densely without coagulation despite the harsh processing conditions (temperature, pressure, high viscosity) and the strong arising shear forces. Although the PPE droplets collide and deform as evident from their nonspherical shape, the JPs at the interface provide efficient stabilization and repulsion for the droplets. The size of most droplets is well below 1 μm as a direct result of efficient reduction of interfacial energy. Despite the excess of PPE in the feed, we still find PPE droplets in a SAN matrix, because the high viscosity ratio, $\eta_{PPE}/\eta_{SAN} > 10$, shifts phase inversion far from a feed ratio of 50/50 (w/w). This peculiarity is well-known for PPE/SAN, where the less viscous SAN always forms the matrix.[32,33] On closer inspection of the droplet morphology in Figure 2b, we frequently observe brighter SAN droplets inside the darker PPE droplets, suggesting a double emulsion morphology, usually found close to phase inversion,[41] *i.e.*, SAN droplets in PPE matrix (see also Supporting Information Figures S4 and S5). The TEM close-up in Figure 2c corroborates the double emulsion morphology. Here, the larger PPE droplet engulfs smaller SAN droplets, while all interfaces are densely covered with JPs visible as black dots (OsO_4 staining of remaining PB double bonds). We will discuss the origin of this morphology and the narrow droplet size distribution in more detail later.

To get a better overview of the blend structures, SEM images of the neat and JP compatibilized blends are shown in Figure 3, panels a and b, respectively. Here again the difference in blend structures shows a clear transition from a random co-continuous structure to a homogeneous droplet structure. The morphological difference is also clearly demonstrated when comparing horizontal (parallel to extrusion direction) and vertical (perpendicular to extrusion direction) fractures of the blends to evaluate the homogeneity throughout

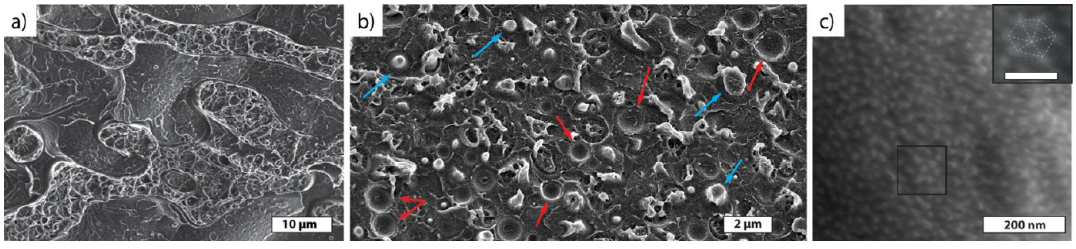

Figure 3. SEM overview of cryo-fractured blends. Irregular shaped neat (a) and compatibilized blend interface with small drop morphology (b). Red and blue arrows point to dents and bumps left behind by pulled-out droplets and remaining droplets, respectively. (c) SEM magnification of a PPE droplet interface fully covered by JPs (raspberry-like structure). The inset is a further magnification of the region marked by the black square and illustrates the hexagonal packing tendency of the JPs at the interface (scale bar in inset is 100 nm).

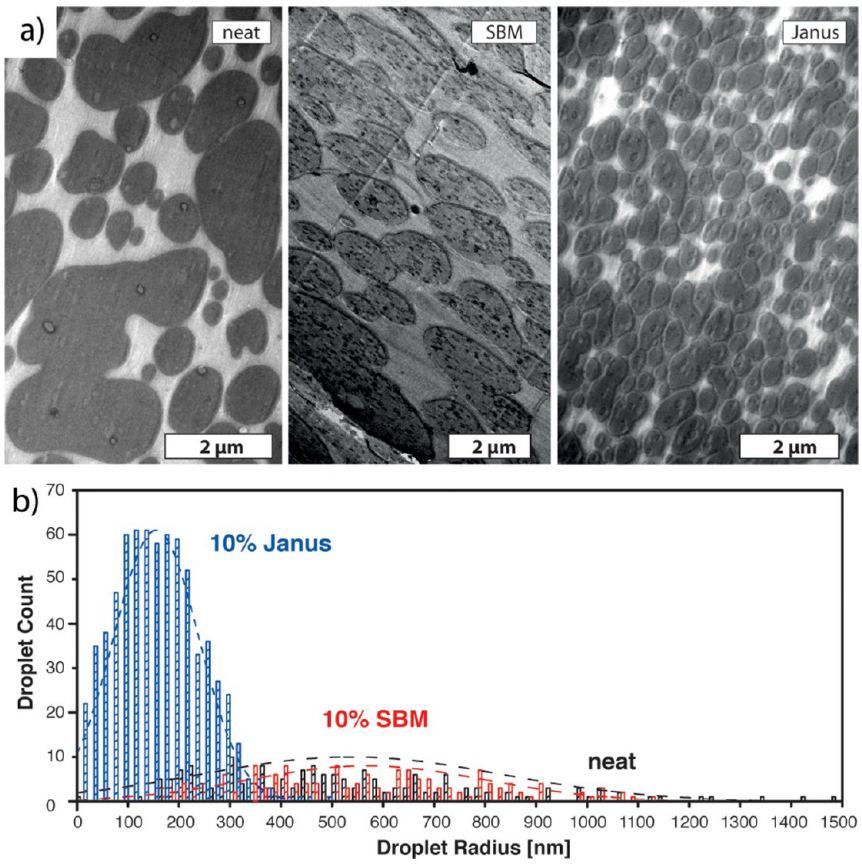

Figure 4. Impact of compatibilizer on blend morphology. (a) TEM images of the neat blend (without additive, perpendicular to the extrusion direction), compatibilized with 10 wt % SBM triblock terpolymer and with 10 wt % SBM JPs (slight contrast differences originate from varying film thicknesses). (b) Histogram of 500 droplet radii for all blend systems.

the samples (Supporting Information Figure S6). The JP blend displays submicrometer features in both directions proving isotropic distribution of the blend components. Compared to that, the neat blend contains micrometer-sized elliptical domains in the horizontal, but distinctly different elongated cylindrical domains in the vertical cross section attributed to anisotropic shearing of the PPE phase. This difference in morphological homogeneity should have profound effects on the stability of the blend when subjected to stress. We find the droplet morphology also in SEM as a random distribution of dents and bumps corresponding to droplets and holes left behind by detached PPE droplets (Figure 3b; red and blue arrows). The droplets show a multiscale structure as they are fully covered with JPs, forming raspberry-like structures in a SAN matrix. We clearly identify the JPs at the blend interface in SEM (Figure 3c). After cryo-fracturing of the blend, the droplet surface is fully decorated with small spherical particles corresponding to points of adhesion between PPE and SAN mediated by JPs. The inset in Figure 3c shows a tendency for hexagonal close packing with interparticle distances of 30 nm attributed to the JP size in the collapsed state (Supporting Information Figure S3).[37]

Although very similar packing was observed previously with a PS/PMMA blend,[27] the PPE/SAN blend inherits a set of entirely different physical properties. The fact that JPs still selectively locate at the interface is remarkable and explained by the energy, ΔE_{desorb}, required to desorb the JPs from the blend interface. According to eq 1 (see Supporting Information),

$$\Delta E_{desorb.} \approx 3\pi R_{JP}^2 \gamma_{PPE/SAN} \quad (1)$$

increases with the square of the particle radius, R_{JP}, and the interfacial tension between the blend components, $\gamma_{PPE/SAN}$.[25,27] The interfacial tension between two polymers can be estimated from the Flory–Huggins polymer–polymer interaction parameter, χ, applying the relation $\gamma \propto \chi^{1/2}$ (for $\chi > 0$). In the studied system, all parameters favor JP location at the interface,[40] *i.e.*, high incompatibility of the blend components, $\chi_{PPE/SAN} > 0.5$, and good compatibility between blend components and the respective JP corona blocks, $\chi_{PPE/PS} = -0.044$ and $\chi_{SAN/PMMA} = -0.008$[31] (for 19 wt % AN in SAN). To further increase $\Delta E_{desorb.}$, we chose JPs to be considerably larger than the radius of gyration of the blended polymers ($R_{g,polymer} < 10$ nm *vs* $R_{JP,TEM} = 19$ nm; $V_{JP}/V_{polymer} \geq 7$). Although an exact calculation of $\Delta E_{desorb.}$ is elusive, the quantitative adsorption of JP to the blend interface suggests that $\Delta E_{desorb.}$ must be sufficiently high to overcome the thermal energy impacting the particles at 260 °C during extrusion.

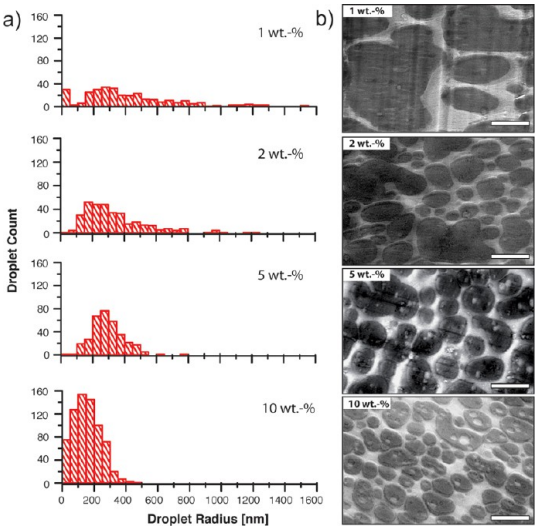

Figure 5. Dependence of droplet size on JP content. (a) Histograms of 500 droplet radii and (b) TEM image series of the corresponding morphologies.

Figure 4 summarizes the efficiency with which the JPs compatibilize this blend system. Here, we compare the morphology without additive, compatibilized with 10 wt % $S_{32}B_{36}M_{32}^{93}$ triblock terpolymer and with 10 wt % JPs made from $S_{40}B_{20}M_{40}^{108}$. All other processing parameters were kept constant to allow reliable comparison. The JPs considerably reduce the droplet size as compared to the neat blend and also significantly outperform the SBM triblock terpolymer (Figure 4a).

For each system we analyzed the radii of 500 PPE droplets in TEM micrographs of ultrathin cuts. The radius of each droplet is calculated from the cross-sectional area (determined using ImageJ software), assuming spherical shape (Figure 4b). The average droplet radius, R_{PPE}, and standard deviation strongly decrease from $R_{PPE;SBM} = 670 \pm 230$ nm to $R_{PPE;JP} = 155 \pm 85$ nm underlining the superior stabilization capabilities of JPs as compared to the SBM triblock terpolymer. Both compatibilizers are amphiphilic in nature and exhibit the same interactions with the blend polymers, which is why we consider the Pickering effect and the accompanying high interfacial activity of the JPs mostly responsible for the significant improvement. The droplet radius for the neat blend, $R_{PPE\text{-}neat} = 540 \pm 300$ nm, was determined for the sake of completeness, but does not adequately reflect the occasional multi micron-sized droplets. Without any additive, the neat blend yields entirely unpredictable and irreproducible morphologies that may change at any given point even within the same extrusion experiment. In addition, reasonable droplet evaluation was complicated by excessive droplet coagulation, commonly observed for insufficient or missing surface stabilization (compare also Figure 2a and 3a). The difference between the SBM triblock terpolymer and the neat blend is surprisingly small. Both show broad distributions without significant shift

TABLE 1. Dependence of Average Droplet Size and Stabilization Efficiency on the JP Content

f_P [wt %]	R_{PPE} [nm][a]	$\sigma(R_{PPE})$ [nm][b]	$R_{PPE}(f_{JP})^{1/2}$ [nm]
0	540	300	-
1	440	350	440
2	340	190	480
5	270	100	600
10	150	80	474

[a] Average of 500 droplets. [b] Standard deviation.

of the average radius. We believe that a considerable fraction of the SBM triblock terpolymer is actually present as micelles or micelle clusters that manifest as black spots inside PPE droplets in Figure 4a (SBM-stabilized blend). These micelles in the SBM compatibilized blends are the reason for reduced efficiency of SBM during compatibilization (probably due to lower interfacial activity compared to JPs). These trapped SBM polymer chains in PPE do not contribute to the stabilization of interfaces. Therefore, the difference between neat and SBM blends is only a more homogeneous morphology without smaller droplet sizes.

Figure 5 and Table 1 illustrate the morphological evolution of the blend as a function of the Janus particle content, *i.e.* at weight fractions of f_{JP} = 0, 1, 2, 5, and 10 wt %. The histograms in Figure 5a show a distinct trend for the evolution of droplet radius in dependence of JP content. The addition of only 0.5 (not shown) and 1 wt % JPs is not able to provide the necessary coverage to stabilize the interface and besides irregular droplet shape and large average droplet radii, droplets still partly coagulate into the co-continuous PPE/SAN morphology (Figure 2a). Figure 5b shows that by increasing the JP content, not only the PPE domain size becomes smaller, but also the homogeneity of the blend morphology improves.

Therefore, the occasional too large or too small particles visible in the blends with 1 and 2 wt % JPs are not visible in blends with 5 and 10 wt % JPs. The homogeneity of the blend morphology would result in homogeneous macro mechanical properties and is of great industrial interest. As already discussed, at f_{JP} = 10 wt % (and at a lower extent in the blend with 5 wt % JP) the morphology is reminiscent of a double emulsion with SAN inclusions inside PPE droplets. We hypothesize that the system creates additional interface due to excess stabilization capability of the large amount of JP added. The second interface also suggests that the droplet already reached its optimum curvature considering the given interfacial energies. Assuming a dense packing of the JPs on the interface area, A_{PPE}, simple geometric relations show that the radius of the PPE droplets should scale with the inverse square root of the JP content, f_{JP}:

$$A_{PPE} = 4\pi R_{PPE}^2 \propto f_{JP}^{-1}$$
$$\therefore R_{PPE} \propto f_{JP}^{-1/2} \text{ or } R_{PPE} \cdot f_{JP}^{1/2} = \text{const.} \quad (2)$$

Table 1 shows that (with the exception of f_{JP} = 5 wt. %) the product $R_{PPE} \cdot f_{JP}^{1/2}$ is indeed constant, confirming our assumption that the JPs densely pack at the interface, irrespective of the JP content.

The SAN inclusions are only visible in the blends with 5 wt % JP or more and are less frequent compared to the significant micelle and micellar cluster formation observed in the SBM compatibilized blend. To understand the formation of the SAN inclusions in the 5 and 10 wt % blends, shear rheology measurements were performed on the neat and the JP compatibilized blends (Figure 6).

The increase in viscosity after the addition of JPs indicates effective compatibilization as a result of enhanced stress transfer between the phases in the blends with f_{JP} = 1, 2, and 5 wt %. In case of the blend with 10 wt % JPs, the viscosity does not change significantly in the high frequency range as compared to the neat blend. However, at lower frequencies, an increase in the viscosity is visible, indicating some network-like structure formations. The 3D network forms through structure buildup of the PPE droplets in the matrix once

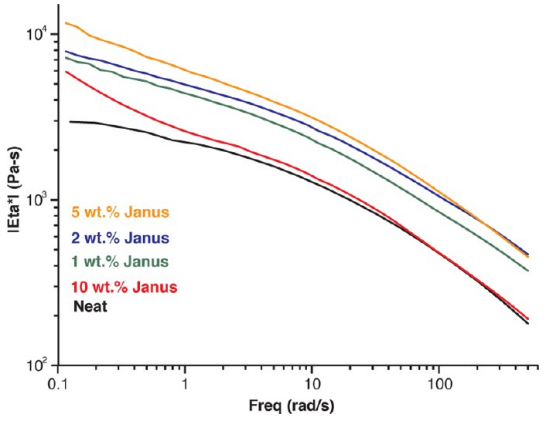

Figure 6. Absolute zero shear viscosities of the PPE/SAN blends compatibilized with 1, 2, 5, and 10 wt % JPs.

their sizes drop below a critical value.[42] We assume that at high JP concentration during extrusion, at first the particles cover all PPE droplet interface and minimize droplet size, while excess JPs are still present as clusters in one of the phases (for equal hemispheres cluster formation is equally probable in both phases). These excess JPs which form clusters (supermicelles) are freely dispersed in the blend, and since they are small spherical particles, they can facilitate low friction sliding between the PPE droplets and the overall viscosity of the blend is reduced to that of the neat blend. In case of the blend with 5 wt % JPs, we observe a similar phenomenon at smaller scale (Figure 5), also corroborating that the most economic amount of Janus particles to realize full compatibilization of the blend is indeed f_{JP} = 2−5 wt %. Another consequence of the excess amounts of JPs in the 5 and 10 wt % blend is that the system tries to build up extra surface to accommodate excess JPs and hence, SAN inclusions form within the PPE droplets. In addition, the lower viscosity of the blend at higher shear rates further facilitates the formation of such SAN inclusions.

Although the effect of processing parameters on the blend morphology has been comprehensively studied in the past, many works conclude that the mechanisms of morphology development and the final morphology would be similar for batch mixers and twin-screw extruders. However, one should always keep in mind that the shear field generated is unique to the equipment and may have different, even dramatic effects on the polymer blend. To study the effect of different shear rates, two processing machines, one with high and one with low shear forces have been chosen to compare the effect of processing conditions on the blend material. At first, all other processing conditions including residence time, temperature profile, and screw speed were kept constant and only the effect of different shear fields was investigated. We blended

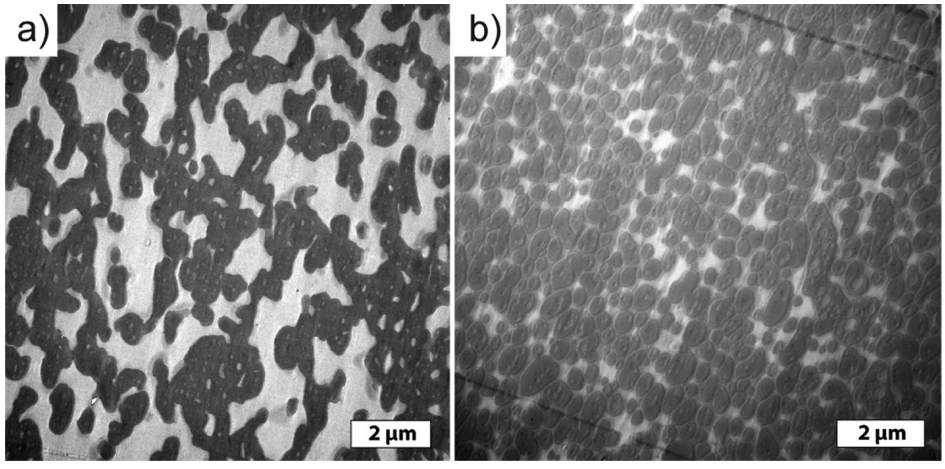

Figure 7. Morphologies obtained for lab- and large-scale compounding of PPE/SAN blends compatibilized with 10 wt % JPs. (a) Co-continuous morphology produced with mini-compounder under low shear conditions and (b) nanosized drop morphology of the same blend composition produced with industry-scale extruder with high shear forces.

PPE/SAN with JP on a lab-scale mini-compounder which produces low shear forces and obtained a co-continuous morphology compared to the industry-scale extruder which has much higher shear forces, demonstrating the profound effect of forces accompanied to the used machinery (Figure 7). The measured torque values during the process were 5 and 45 Nm for mini-compounder and extruder, respectively, which confirm low and high shear forces during the process. Since it is here proven that low shear forces in the mini compounder cannot break up the high viscous PPE phase into droplets, another experiment was performed with higher mixing (residence) time. From the results (Supporting Information Figure S7), one can conclude that the effect of shear forces produced by the machine is much higher than that of processing conditions (such as residence time), since the blend with double residence time in the compounder still shows co-continuous morphology. This is because mechanisms leading to PPE droplet break up need high shear forces and, within the steady state regime, are independent of residence time. This knowledge is of particular interest when designing and testing lab-scale prototype materials or working with special blend systems (*i.e.*, with high viscosity ratios). In case of some polymer blends with special viscosity ratios, extensional flows are needed to provide the desired morphologies and therefore, other compounding devices such as co-kneader twin-screw extruders would be needed. To predict morphologies in blends, the underlying mechanisms need to be understood more clearly, which is why we are convinced that large-scale studies establish an invaluable basis for the application-oriented development of designer materials (such as JPs) and likewise for the advancement of existing theoretical models.

CONCLUSIONS

We demonstrated the efficient compatibilization of PPE/SAN blends using Janus nanoparticles in industry-scale blending equipment. The combination of strong interfacial affinity and the Pickering effect promote quantitative adsorption of JPs to the blend interface irrespective of the harsh processing conditions. The Pickering effect significantly contributes to particle adsorption by overcoming the high thermal energy of the particles in the polymer melt. The optimum fraction of JPs necessary for sufficient droplet stabilization without formation of double emulsion morphology was determined to be in the range of 2−5 wt %. A more economic use of the Janus nanoparticles may be realized by admixing specific amounts of SBM triblock terpolymer. Preliminary results show synergetic stabilization capabilities of SBM JPs/triblock terpolymer mixtures. Entirely different morphologies were obtained for lab-scale and industry-scale processing underlining the importance of large-scale studies on systems involving specialized materials. Ongoing work comprises comprehensive studies on mechanical properties, the use of Janus nanoparticles with unequal-sized volume ratios of the corona hemispheres (Janus balance), and synergetic effects of JPs in combination with other conventional compatibilizers. Especially JPs with Janus balance in favor of the stabilizing patch could result in even smaller droplet radii than the ones reported.

EXPERIMENTAL SECTION

Materials. All solvents used were of analytical grade. Dialysis tubes of regenerated cellulose with a MWCO of 12 000−14 000 g/mol were purchased from Roth, equilibrated in deionized water for 30 min and washed with excess dioxane before use. The photo-cross-linker, 2,4,6-trimethylbenzoyldiphenylphosphineoxide ($\lambda_{max} \approx 360$ nm) was obtained from BASF AG, Ludwigshafen, Germany (Lucirin TPO). Commercial-grade poly(2,6-dimethyl-1,4-phenylene ether) (PPE; PX100F) was obtained as powder from Mitsubishi Engineering Plastics Europe, Düsseldorf, Germany. The weight-average molecular weight M_w = 12.9 kg/mol and the polydispersity index PDI = 1.63 of PPE was determined by size exclusion chromatography (SEC) with THF as eluent at a flow rate of 1.0 mL/min (columns at 40 °C) using an UV detector and polystyrene standards for calibration. The commercially available poly(styrene-*co*-acrylonitrile) (SAN) with a acrylonitrile content of 19 wt % was purchased as pellets, from BASF AG, Ludwigshafen, Germany (SAN VLL 19100). The M_w = 97.1 kg/mol and PDI = 2.13 of SAN was determined the same way as mentioned above. The low acrylonitrile content of the polymer ensures homogeneous miscibility of the SAN with the PMMA blocks of the compatibilizers at the relevant processing conditions. Irganox 1010 and Irgafos 168 (BASF, Germany) were used as stabilizers to prevent polymer heat degradation during the process.

Synthesis of SBM Janus Nanoparticles. The SBM triblock terpolymers were synthesized *via* sequential living anionic polymerization of styrene, butadiene and methyl methacrylate, as reported elsewhere in detail.[32] The Janus nanoparticles were prepared according to a recipe modified from the earlier report to satisfy the requirements of industry blending equipment.[37] In a typical experiment, 100 g of SBM triblock terpolymer was dissolved in 1 L THF to yield a concentration of c = 100 g/L. After complete dissolution, the concentrated polymer solution was dialyzed against 10 L acetone/2-propanol (60/40 v/v) (selective solvent for PMMA). The solvent mixture was changed twice to generate JPs clusters (spherical multicompartment micelles that consist of JPs). After dialysis, the phase-separated state of the micelles was permanently fixed by cross-linking of the PB block. Therefore, 0.25 equiv (compared to the PB double bonds) of photo-cross-linker, 2,4,6-trimethylbenzoyldiphenylphosphineoxide (Lucirin TPO; $\lambda_{max} \approx 360$ nm) was dissolved in 1 L acetone/2-propanol (60/40 v/v) and added to the dispersion of the JPs clusters to dilute the highly viscous dispersion from 100 to 50 g/L. The sample was then irradiated for 24 h using a UV-lamp with a cutoff filter of λ = 300 nm. Continuous stirring ensured homogeneous cross-linking of the opaque solution. The Janus micelles were recovered by precipitation into 20 L methanol.

Preblending of Dry Polymer Powders. Before melt blending of the homopolymers, the PPE powder and the SAN pellets were dried at 80 °C for at least 12 h under vacuum. For SBM triblock terpolymers and JPs a lower temperature of 40 °C was chosen due to sensitivity of the PB block to degradation when longer exposed to oxygen atmosphere at elevated

temperatures. In addition, the SBM and Janus compatibilizers were cryo-grinded into a powder. Prior to melt blending, PPE and SAN were dry blended with SBM or JPs using powder mixers. The PPE/SAN ratio was kept constant at 60/40; however, for each blend, the amount of compatibilizer (SBM or Janus particles) was varied to 0.5, 1.0, 2.0, and 10 wt %. To prevent thermal degradation, 0.1 wt % of stabilizer (mixture of Irganox 1010 and Irgafos 168) was added to the compounds.

Instrumentation. *Lab-Scale Melt Processing.* Melt blending of the compounds was performed on a microcompounder (Xplore DSM) with co-rotating conical twin-screw setup and volume capacity of 15 mL. This process is comparable to a batch mixing process. The temperature inside the microcompounder was kept constant at 260 °C, the screw speed at 85 rpm and the mixing time was 5 min (similar to the residence time in the extruder). The melt strands were cooled and cut into pellets.

Industry-Scale Melt Processing. A continuous scale, co-rotating twin-screw extruder (Brabender DSE 20/40) with L/D = 30 was used to compound the polymer blends. The maximum barrel and nozzle temperature were fixed at 250 and 245 °C, respectively, and the screw speed was kept constant at 85 rpm with a constant throughput of 1 kg/h. Therefore, the mean residence time of the blends in the extruder was around 5 min.

Transmission Electron Microscopy (TEM). Ultrathin sections (60 nm) were cut of the blended materials at room temperature using an ultramicrotome (Reichert-Jung Ultracut E microtome) equipped with a diamond knife. Micellar samples were prepared by placing one drop of the polymer solution (0.01 g/L) onto carbon-coated copper grids. Excess solvent was instantly absorbed by a filter paper. To ensure sufficient contrast between the phases, the particles and ultrathin sections were stained with OsO_4 for 30 s in vacuum in case of SBM compatibilized blends and 3 h at ambient conditions in case of Janus particle compatibilized blends. Due to this staining method, SAN appears as the brighter and PPE as the darker phase, while the PB block (or core) of SBM (JPs) appears black (selectively stained with OsO_4). Bright field transmission electron microscopy at an acceleration voltage of 80 kV was carried out using a Zeiss CEM 902 electron microscope. Number-average diameter of the PPE droplets and their distribution were obtained by measuring 500 droplets in TEM micrographs using ImageJ software. First, the area of each PPE droplet was measured using the software; then, assuming that droplets are fully spherical particles and the TEM cuts have gone through middle of each droplet, the radius corresponding to the area was back calculated. Of course these assumptions cannot be 100% fulfilled, hence resulting in the relatively large standard deviations in Table 1.

Field Emission Scanning Electron Microscopy (FESEM) was conducted on a Leo 1530 Gemini from Zeiss using a secondary electron detector and an acceleration voltage of 15 kV. For a better contrast, the samples were sputtered with a 1.3 nm thick platinum layer.

Dynamic Light Scattering (DLS) was performed at a scattering angle of 90° on an ALV DLS/SLS-SP 5022F equipment consisting of an ALV-SP 125 laser goniometer, an ALV 5000/E correlator, and a He−Ne laser operating at a wavelength of $\lambda = 632.8$ nm. The CONTIN algorithm was applied to analyze the obtained correlation functions. Apparent hydrodynamic radii were calculated according to the Stokes−Einstein equation. All CONTIN plots are intensity-weighted. Prior to the light scattering measurements, all sample solutions were filtered twice through a 5 μm PTFE-filter.

Rheological Investigations. Rheological properties were investigated by a stress controlled dynamic-mechanical rheometer RDA III from Rheometric Scientific with plate−plate geometry under nitrogen atmosphere. The pressed samples had a diameter of 25 mm and thickness of 1.5 mm and were analyzed isothermally at 260 °C. The storage modulus, the loss modulus, and the complex viscosity of blend systems were measured as a function of frequency within the range of 0.01−500 rad/s at 260 °C. Prior to each measurement, the linear viscoelastic region was determined by carrying out an amplitude sweep at a deformation range of 0.1−100%, at frequencies of 1 and 50 rad/s. Subsequently, the deformation applied for the frequency sweeps was set to be within the linear viscoelastic region. Each measurement was repeated at least three times to minimize the experimental errors.

Conflict of Interest: The authors declare no competing financial interest.

Supporting Information Available: Additional experimental data; SEC and TEM characterization of SBM; additional TEM and SEM images of blends; supporting calculations and Figures S1−S7. This material is available free of charge *via* the Internet at http://pubs.acs.org.

Acknowledgment. This work was supported by the Deutsche Forschungsgemeinschaft within grants AL 474/21-1 and Mu 896/39-1. The authors acknowledge BASF for donating SAN and Mitsubishi for PPE polymer.

REFERENCES AND NOTES

1. Leibler, L. Nanostructured Plastics: Joys of Self-Assembling. *Prog. Polym. Sci.* **2005**, *30*, 898–914.
2. Paul, D. R.; Bucknall, C. B. *Polymer Blends*; Wiley: New York, 2000.
3. Utracki, L. A. *Commercial Polymer Blends*; 1st ed.; Chapman and Hall: London, 1998.
4. Pernot, H.; Baumert, M.; Court, F.; Leibler, L. Design and Properties of Co-Continuous Nanostructured Polymers by Reactive Blending. *Nat. Mater.* **2002**, *1*, 54–58.
5. Kietzke, T.; Neher, D.; Landfester, K.; Montenegro, R.; Güntner, R.; Scherf, U. Novel Approaches to Polymer Blends Based on Polymer Nanoparticles. *Nat. Mater.* **2003**, *2*, 408–412.
6. Macosko, C. W.; Gue, P.; Khandpur, A. K.; Nakayama, A.; Marechal, P.; Inoue, T. Compatibilizers for Melt Blending: Premade Block Copolymers. *Macromolecules* **1996**, *29*, 5590–5598.
7. Cerclé, C.; Favis, B. D. Generalizing Interfacial Modification in Polymer Blends. *Polymer* **2012**, *53*, 4338–4343.
8. Cai, X.; Li, B.; Pan, Y.; Wu, G. Morphology Evolution of Immiscible Polymer Blends as Directed by Nanoparticle Self-Agglomeration. *Polymer* **2012**, *53*, 259–266.
9. Kim, B. J.; Bang, J.; Hawker, C. J.; Chiu, J. J.; Pine, D. J.; Jang, S. G.; Yang, S.-M.; Kramer, E. J. Creating Surfactant Nanoparticles for Block Copolymer Composites through Surface Chemistry. *Langmuir* **2007**, *23*, 12693–12703.
10. Jang, S. G.; Kramer, E. J.; Hawker, C. J. Controlled Supramolecular Assembly of Micelle-like Gold Nanoparticles in PS-b-P2VP Diblock Copolymers *via* Hydrogen Bonding. *J. Am. Chem. Soc.* **2011**, *133*, 16986–16996.
11. Zhao, Y.; Thorkelsson, K.; Mastroianni, A. J.; Schilling, T.; Luther, J. M.; Rancatore, B. J.; Matsunaga, K.; Jinnai, H.; Wu, Y.; Poulsen, D.; et al. Small-Molecule-Directed Nanoparticle Assembly towards Stimuli-Responsive Nanocomposites. *Nat. Mater.* **2009**, *8*, 979–985.
12. Cao, Y.; Zhang, J.; Feng, J.; Wu, P. Compatibilization of Immiscible Polymer Blends Using Graphene Oxide Sheets. *ACS Nano* **2011**, *5*, 5920–5927.
13. Du, B.; Handge, U. A.; Majeed, S.; Abetz, V. Localization of Functionalized MWCNT in SAN/PPE Blends and Their Influence on Rheological Properties. *Polymer* **2012**, *53*, 5491–5501.
14. Balazs, A. C.; Emrick, T.; Russell, T. P. Nanoparticle Polymer Composites: Where Two Small Worlds Meet. *Science* **2006**, *314*, 1107–1110.
15. Kao, J.; Thorkelsson, K.; Bai, P.; Rancatore, B. J.; Xu, T. Toward Functional Nanocomposites: Taking the Best of Nanoparticles, Polymers, and Small Molecules. *Chem. Soc. Rev.* **2013**, *42*, 2654–2678.
16. Duin, V. A. N.; Jerome, R. Strategies for Compatibilization of Polymer Blends. *Prog. Polym. Sci.* **1998**, *23*, 707–757.
17. Li, G.; Shrotriya, V.; Huang, J.; Yao, Y.; Moriarty, T.; Emery, K.; Yang, Y. High-Efficiency Solution Processable Polymer Photovoltaic Cells by Self-Organization of Polymer Blends. *Nat. Mater.* **2005**, *4*, 864–868.
18. Walther, A.; Hoffmann, M.; Müller, A. H. E. Emulsion Polymerization Using Janus Particles as Stabilizers. *Angew. Chem., Int. Ed.* **2008**, *47*, 711–714.

19. Gröschel, A. H.; Löbling, T. I.; Petrov, P. D.; Müllner, M.; Kuttner, C.; Wieberger, F.; Müller, A. H. E. Janus Micelles as Effective Supracolloidal Dispersants for Carbon Nanotubes. *Angew. Chem., Int. Ed.* **2013**, *52*, 3602–3606.
20. Kim, S.-H.; Lee, S. Y.; Yang, S.-M. Janus Microspheres for a Highly Flexible and Impregnable Water-Repelling Interface. *Angew. Chem., Int. Ed.* **2010**, *49*, 2535–2538.
21. Hirsemann, D.; Shylesh, S.; De Souza, R. A; Diar-Bakerly, B.; Biersack, B.; Mueller, D. N.; Martin, M.; Schobert, R.; Breu, J. Large-Scale, Low-Cost Fabrication of Janus-Type Emulsifiers by Selective Decoration of Natural Kaolinite Platelets. *Angew. Chem., Int. Ed.* **2012**, *51*, 1348–1352.
22. Walther, A.; Müller, A. H. E. Janus Particles: Synthesis, Self-Assembly, Physical Properties, and Applications. *Chem. Rev.* **2013**, *113*, 5194–5261.
23. Wurm, F.; Kilbinger, A. F. M. Polymeric Janus Particles. *Angew. Chem., Int. Ed.* **2009**, *48*, 8412–8421.
24. Jiang, S.; Chen, Q.; Tripathy, M.; Luijten, E.; Schweizer, K. S.; Granick, S. Janus Particle Synthesis and Assembly. *Adv. Mater.* **2010**, *22*, 1060–1071.
25. Binks, B. P.; Fletcher, P. D. I. Particles Adsorbed at the Oil - Water Interface: A Theoretical Comparison between Spheres of Uniform Wettability and " Janus " Particles. *Langmuir* **2001**, 4708–4710.
26. Kim, J.; Matsen, M. Positioning Janus Nanoparticles in Block Copolymer Scaffolds. *Phys. Rev. Lett.* **2009**, *102*, 078303.
27. Walther, A.; Matussek, K.; Müller, A. H. E. Engineering Nanostructured Polymer Blends with Controlled Nanoparticle Location Using Janus Particles. *ACS Nano* **2008**, *2*, 1167–1178.
28. Xu, K.; Guo, R.; Dong, B.; Yan, L.-T. Directed Self-Assembly of Janus Nanorods in Binary Polymer Mixture: Towards Precise Control of Nanorod Orientation Relative to Interface. *Soft Matter* **2012**, *8*, 9581–9588.
29. Yan, L.-T.; Popp, N.; Ghosh, S.-K.; Böker, A. Self-Assembly of Janus Nanoparticles in Diblock Copolymers. *ACS Nano* **2010**, *4*, 913–920.
30. Huang, M.; Li, Z.; Guo, H. The Effect of Janus Nanospheres on the Phase Separation of Immiscible Polymer Blends *via* Dissipative Particle Dynamics Simulations. *Soft Matter* **2012**, *8*, 6834–6845.
31. Merfeld, G. D.; Karim, A.; Majumdar, B.; Satija, S. K.; Paul, D. R. Interfacial Thickness in Bilayers of Poly(phenylene oxide) and Styrenic Copolymers. *J. Polym. Sci.* **1998**, *36*, 3115–3125.
32. Ruckdäschel, H.; Sandler, J. K. W.; Altstädt, V.; Rettig, C.; Schmalz, H.; Abetz, V.; Müller, A. H. E. Compatibilisation of PPE/SAN Blends by Triblock Terpolymers: Correlation between Block Terpolymer Composition, Morphology and Properties. *Polymer* **2006**, *47*, 2772–2790.
33. Ruckdäschel, H.; Sandler, J. K. W.; Altstädt, V.; Schmalz, H.; Abetz, V.; Müller, A. H. E. Toughening of Immiscible PPE/SAN Blends by Triblock Terpolymers. *Polymer* **2007**, *48*, 2700–2719.
34. Ruckdäschel, H.; Gutmann, P.; Altstädt, V.; Schmalz, H.; Müller, A. H. E. Foaming of Microstructured and Nanostructured Polymer Blends. In *Advances in Polymer Science*; Springer-Verlag: Berlin Heidelberg, 2010.
35. Kirschnick, T.; Gottschalk, A.; Ott, H.; Abetz, V.; Puskas, J.; Altstädt, V. Melt Processed Blends of Poly(styrene-co-acrylonitrile) and Poly(phenylene ether) Compatibilized with Polystyrene-b-Polybutadiene-b-Poly(methyl methacrylate) Triblock Terpolymers. *Polymer* **2004**, *45*, 5653–5660.
36. Loget, G.; Roche, J.; Kuhn, A. True Bulk Synthesis of Janus Objects by Bipolar Electrochemistry. *Adv. Mater.* **2012**, *24*, 5111–5116.
37. Gröschel, A. H.; Walther, A.; Löbling, T. I.; Schmelz, J.; Hanisch, A.; Schmalz, H.; Müller, A. H. E. Facile, Solution-Based Synthesis of Soft, Nanoscale Janus Particles with Tunable Janus Balance. *J. Am. Chem. Soc.* **2012**, *134*, 13850–13860.
38. Dobkowski, Z. Determination of Critical Molecular Weight for Entangled Macromolecules Using the Tensile Strength Data. *Rheol. Acta* **1995**, *34*, 578–585.
39. Wool, R. P. *Polymer Interfaces*; 1st ed.; Carl Hanser: Munich, 1995.
40. Stadler, R.; Auschra, C.; Beckmann, J.; Krappe, U.; Voigt-Martin, I.; Leibler, L. Morphology and Thermodynamics of Symmetric Poly (A-block-B-block-C) Triblock Copolymers. *Macromolecules* **1995**, *28*, 3080–3091.
41. Macosko, C. W. Morphology Development and Control in Immiscible Polymer Blends. *Macromol. Symp.* **2000**, *149*, 171–184.
42. Münstedt, H. Rheology of Rubber-Modified Polymer Melts. *Polym. Eng. Sci.* **1981**, *21*, 259–270.